

Original Article

## Computational one-factor investigation on the effect of sonication parameters in biomass pretreatment



Wah Yen Tey<sup>1,2,\*</sup> , Kiat Moon Lee<sup>3</sup> 

<sup>1</sup> Department of Mechanical Engineering, Faculty of Engineering, UCSI University, Kuala Lumpur, Malaysia.

<sup>2</sup> Takasago i-Kohza, Malaysia-Japan International Institute of Technology, Universiti Teknologi Malaysia Kuala Lumpur, Kuala Lumpur, Malaysia.

<sup>3</sup> Department of Chemical and Petroleum Engineering, Faculty of Engineering, UCSI University, Kuala Lumpur, Malaysia.

### Abstract

The application of ultrasonic irradiation has been proven as a clean and efficient approach for biomass pretreatment process. However, the effects of sonication parameters on the performance of biomass pretreatment are not well discussed due to its physical complexity. The current work aims to model Rayleigh-Plesset equation (RPE) to investigate how the fluid property of biomass-water (surface tension and dynamic viscosity) and sonication parameters (sonication frequency and power) influence the growth and bounce of microbubbles. The collapsing temperature, collapsing pressure, and shock pressure are computed. Moving Least Squares and Multivariable Power Least Squares Method are applied for multivariate investigation. The results revealed that fluid properties are more significant than sonication parameters.

Copyright © 2021 PENERBIT AKADEMIKA BARU - All rights reserved

### Article Info

Received 13 December 2020

Received in revised form 21 January 2021

Accepted 21 January 2021

Available online 22 January 2021

### Keywords

Ultrasonic irradiation

Biomass energy

Rayleigh-Plesset equation

Moving least squares method


Multivariable power least squares method

## 1 Introduction

Lignocellulosic biomass is one of the promising renewable feedstocks for production of biofuels and biomaterials. Lignocellulosic biomass comprises of lignin, cellulose, and hemicellulose, while these macromolecules are strongly bind together to form a highly crystalline biomass structure, making the biomass recalcitrant to bioprocessing. Destruction of the biomass structure is necessary to expose the cellulosic materials. There are many pretreatment methods available and they can be categorised into physical, chemical, physicochemical, biological and any combination of these pretreatments.

A green and efficient pretreatment method with low cost and easy-to-operate is of great interest in biomass conversion. Recently, ultrasound has applied in biomass pretreatment [1–4]. Ultrasound is mechanical acoustic wave with frequency ranging from 20 kHz to 20 MHz [5]. Ultrasound works based on the principle of acoustically induced cavitation of micro-sized bubbles. When ultrasonic wave passes through a liquid medium, the liquid atoms will oscillate locally in tandem with periodic rarefaction of propagating wave, allowing the formation of transient and stable cavitation bubbles. These bubbles will grow and become unstable and collapse. During the implosion, a high speed microjet of greater than 200 ms<sup>-1</sup> [5,6] is produced and a strong shockwave of pressure up to 103 MPa [6–8] is formed.

The pressure and temperature hike of the collapsing of microbubble could break the chemical bonds of polymeric biomass structure via two mechanisms: sonoluminescence and mechano-acoustical shearing. Sonoluminescence is dominated by the temperature hike, in which the collapsing bubbles will disintegrate the biomass-water atoms into free radicals. These free radicals will further induce micro-combustion reaction which would chemically disrupt the biomass cellulosic walls. Meanwhile, mechano-

\* Corresponding author [teywy@ucsiuniversity.edu.my](mailto:teywy@ucsiuniversity.edu.my) 

acoustical shearing is generated from the sharp increase of pressure, which generate a very strong shear force to mechanically destroy the cell walls. Occasionally, both mechanisms might couple within each other, bolstering the shockwave emission. Some relevant studies on these can be found in the work of Brennen [9], Merouani et al. [10], and Yasui [11].

There are many works reported to incorporate ultrasound in chemical pretreatments such as acid, alkaline, organosolv, ionic liquid and deep eutectic solvent (DES) [3,12–15] in view of their better reaction rate. For instance, cellulose saccharification rate was greatly improved for ultrasound-assisted ionic liquid pretreatment compared to traditional heating at 110°C [16]. There are several factors influencing the performance of biomass pretreatment in ultrasound-assisted pretreatment. They might include reaction temperature, sonication power, sonication frequency, irradiation distance, ultrasonic amplitude, probe diameter, vibration pulse, and physical properties of the reaction medium such as dynamic viscosity and surface tension.

The investigation on the effects of various factors on the efficiency of ultrasonic pretreatment is seminal in optimising the cleaner production. There have been a lot of experimental works reported on the optimisation of ultrasonic pretreatment of biomass, in which most of the experimental works deploy the well-known Response Surface Methodology [17]. The optimised operating conditions are different according to the types of biomass compounds to be pretreated. For instance, Martínez-Patiño et al. [18] investigated the optimisation for extraction of biomass from olive tree based on factors of ethanol concentration, ultrasonic power, and time, and they discovered that the best phenolic compound extraction can be observed at around 55% concentration with 280 W in 15 minutes. Meanwhile Fakayode et al. [19] included ultrasonic solid-to-liquid ratio, power, temperature, frequency, and time in their study, and optimal delignification is obtained at the condition of 180 W and 60 kHz within 40 mins, with ignorable effects from solid-to-liquid ratio.

There are some computational works reporting on the investigation of how these factors influence the pretreatment efficiency. For example, Merouani et al. [20] conducted a preliminary simulation on the effects of ultrasound frequency and acoustic amplitude on ultrasonic pretreatment. Another related work was reported by Sajjadi et al. [21] who numerically analysed the effects of various ultrasonic operating conditions on the chemical reactions for biodiesel synthesis. Meanwhile, Tey et al. [22] simulated how the sound interference could affect the growth and collapse of microbubble. Nonetheless, most of the simulation studies are limited to one-factor mathematical analysis and excluding parametric optimisation.

The purpose of the study is to simulate and optimise the effect of pretreatment factors on ultrasonic cavitation. Four main factors to be included in current study are: (a) surface tension of biomass-water; (b) dynamic viscosity of biomass-water; (c) sonication frequency; and (d) sonication power. The simulation can be conducted based on the well-known Rayleigh-Plesset Equation, while its parametric optimisation is performed using a combination scheme of Moving Least Squares (MLS) and Multivariable Power Least Squares (MPLS) Method.

## 2 Numerical Methodology

### 2.1 Mathematical and Numerical Models

The ultrasonic cavitation is governed by Rayleigh-Plesset Equation (RPE), which can be derived from the Continuity and Navier-Stokes Equation [22]. RPE can be mathematically expressed as in Eq. (1):

$$R \frac{\partial \dot{R}}{\partial t} + \frac{3}{2} \dot{R}^2 = \frac{1}{\rho_\infty} \left[ P_v + P_g \left( \frac{R_0}{R} \right)^{3\eta} - P(t) - \frac{2\sigma_s}{R} - \frac{4\mu\dot{R}}{R} \right] \quad (1)$$

where  $R$ ,  $\rho_\infty$ ,  $P_v$ ,  $P_g$ ,  $R_0$ ,  $\eta$ ,  $\sigma_s$ , and  $\mu$  is the bubble radius, density of biomass-water, vapour pressure, gas pressure, initial bubble radius, ratio of thermal constants ( $C_p/C_v$ ), surface tension of biomass-water, and dynamic viscosity of biomass-water, respectively.  $\dot{R}$  refers to the first derivatives of bubble radius in terms of time, and it can be perceived as velocity of bubble growth/collapse. Meanwhile,  $P(t)$  is the acoustical pressure fluctuation generated by the source of ultrasound, which can be represented by a sinusoidal equation:

$$P(t) = P_\infty + P_A \sin(2\pi ft) \quad (2)$$

where  $P_\infty$ ,  $P_A$ ,  $f$  and  $t$  are atmospheric pressure, amplitude of acoustical pressure emitted, ultrasonic frequency, and time, respectively. The amplitude of acoustical pressure can be related with the ultrasonic power  $W$  using Eq. (3):

$$P_A = \sqrt{\frac{W \rho_\infty c^2}{A}} \quad (3)$$

with  $A$  is area of ultrasonic irradiation (i.e. ultrasonic probe), while  $c$  is the speed of sound within the biomass-water. The initial bubble radius and initial bubble growth/collapse speed is set as  $R_0 = 1 \times 10^{-6}$  m and  $\dot{R} = 0$  m/s, respectively. In current study, the value of the parameters involved is summarised in Table 1.

**Table 1** Value of pretreatment parameters involved in current study.

Parameter	Value
Ratio of thermal constants $\eta$	1.4
Speed of sound $c$	1450 m/s
Gas pressure $P_g$	0.4 kPa
Vapour pressure $P_v$	10 kPa
Atmospheric pressure $P_\infty$	101.325 kPa
Area of ultrasonic irradiation $A$	0.1 m <sup>2</sup>
Biomass-water density $\rho_\infty$	1000 kg/m <sup>3</sup>
Biomass-water surface tension $\sigma_s$	$50 \times 10^{-3} \text{ N/m} \leq \sigma_s \leq 350 \times 10^{-3} \text{ N/m}$
Biomass-water dynamic viscosity $\mu$	$0.2 \times 10^{-3} \text{ Pa.s} \leq \mu \leq 1.4 \times 10^{-3} \text{ Pa.s}$
Ultrasonic frequency $f$	$20 \text{ kHz} \leq f \leq 140 \text{ kHz}$
Ultrasonic power $W$	$100 \text{ W} \leq W \leq 700 \text{ W}$

Eq. (1) can be discretised using Delfim-Soares time integration scheme which has been well explained in the previous work [22,23]. Cash-Karp Runge-Kutta (CKRK) method [24] is then deployed to solve the discretised ordinary differential equation. CKRK method can be written as in Eq. (4). In RPE, a critical sharp change of bubble radius is omnipresent during the collapse and re-formation of the microbubble, and thus the application of constant time step is impractical. A modified adaptive time marching scheme as proposed in previous work [22] is applied, in which the time step can be expressed in a very simple way as a function of instantaneous bubble radius and its associating time index  $\alpha$ , as shown in Eq. (5). The minimum value of  $\alpha$  for computation using CKRK method is 1.6 [22]. In current work, the value of  $\alpha$  is assumed to be 1.95 is assumed.

$$\dot{R}(t_{i+1}) = \dot{R}(t_i) + \Delta t \left( \frac{2825}{27648} k_1 + \frac{18575}{48384} k_3 + \frac{13525}{55296} k_4 + \frac{227}{14336} k_5 + \frac{1}{4} k_6 \right) \quad (4)$$

where

$$k_1 = f(t_i, \dot{R}^n)$$

$$k_2 = f\left(t_i + \frac{\Delta t}{5}, \dot{R}^n + \frac{k_1}{5}\right)$$

$$k_3 = f\left(t_i + \frac{3}{10} \Delta t, \dot{R}^n + \frac{3k_1 + 9k_2}{40}\right)$$

$$k_4 = f\left(t_i + \frac{3}{5} \Delta t, \dot{R}^n + \frac{3k_1 - 9k_2 + 12k_3}{10}\right)$$

$$k_5 = f\left(t_i + \Delta t, \dot{R}^n + \frac{-11k_1 + 135k_2 - 140k_3 + 70k_4}{54}\right)$$

$$k_6 = f\left(t_i + \frac{7}{8}\Delta t, \dot{R}^n + \frac{1631k_1 + 18900k_2 + 2296k_3 + 22137.5k_4 + 3415.5k_5}{55296}\right)$$

$$\Delta t(t_i) = [R(t_i)]^\alpha \quad (5)$$

The sonochemical reaction is dominated by the temperature hike during the collapse of micro bubble  $T_{collapse}$  [25], which can be calculated using Eq. (6). Meanwhile, for mechano-acoustical disruption, bubble collapsing pressure  $P_{collapse}$  [25] and shock pressure  $P_{shock}$  [26] can be obtained via Eq. (7) and Eq. (8) respectively. The effects of biomass-water surface tension, biomass-water dynamic viscosity, sonication frequency, and sonication power on  $T_{collapse}$ ,  $P_{collapse}$ , and  $P_{shock}$  will be investigated in the current study.

$$T_{collapse} = T_\infty \left(\frac{R_{max}}{R}\right)^{3(\eta-1)} \quad (6)$$

$$P_{collapse} = \left[ P_v + P_g \left(\frac{R_0}{R_{max}}\right)^3 \right] \left(\frac{R_{max}}{R}\right)^{3\eta} \quad (7)$$

$$P_{shock} = c_1 \rho_\infty u_s \left[ 10^{(u_s - c)/c_2} - 1 \right] + P_\infty \quad (8)$$

In Eq. (8),  $u_s$  is the shock front velocity (bubble collapse-and-rebound velocity). The value of  $c_1$  and  $c_2$  are equivalent to 5190 m/s and 25306 m/s respectively, according to the experimental validation by Rice and Walsh [27].  $R_0$  is the ambient radius, which can be approximated using linear interpolation method based on the value reported by Merouani et al. [28].

## 2.2 Interpolation Techniques

The computed results can be interpolated using Moving Least Squares (MLS) and Multivariable Power Least Squares (MPLS) method. MLS method was introduced by Lancaster and Salkauskas [29] as a robust interpolation scheme for generation of smooth surface. The method is popular in improvising the finite element scheme to deal with moving boundary problems [30,31]. Due to its mathematical flexibility, MLS method is excellent in interpolation of complex data [32,33]. The details of its mathematical formulation can be referred to the work of Liu and Gu [34]. Meanwhile, MPLS method was proposed in our earlier work [35] as a complementary tool for RSM. Moreover, in MPLS method, the application of normalised value of manipulated factors for the interpolation scheme will produced a normalised MPLS equation, which will render important information on the significance of the factors. The mathematical formulation of both methods will be briefly discussed in the following subsections.

### 2.2.1 Moving Least Squares (MLS) Method

Interpolation using MLS method will lead to the formation of polynomial equations such that:

$$y^h = a_1 P_1 + a_2 P_2 + \dots + a_m P_m = \sum_{j=1}^m P_j(\mathbf{x}) a_j = \mathbf{P}^T \mathbf{a} \quad (9)$$

where  $y^h$ ,  $P$ ,  $a$ , and  $m$  is the interpolated data, polynomial interpolant, its associating coefficients, and maximum number of interpolants prescribed. By taking the least squares procedure on the weighted residuals as in Eq. (10), the unknowns of  $a$  can be obtained by solving the matrix as in Eq. (11).

$$J = \sum_{i=1}^n W_i \left[ \left( \sum_{j=1}^m (P_j(\mathbf{x}) \alpha_j) \right)_i - y_i \right]^2 \quad (10)$$

$$\mathbf{a} = \mathbf{A}^{-1} \mathbf{B} \quad (11)$$

where

$$W_i = 1 - 6r_i^2 + 8r_i^3 - 3r_i^4 \text{ with } r_i = \frac{|x_i - \mathbf{x}|}{\|\mathbf{x}\|} \quad (12)$$

$$\mathbf{A} = \sum_{i=1}^n W_i P_i(x_i) P_i^T(x_i) \quad (13)$$

$$\mathbf{B} = W_i P_i(x_i) \quad (14)$$

The details and a current review of MLS method can be referred in our previous work [36].

### 2.2.2 Multivariable Power Least Squares (MPLS) Method

In contrast with MLS method, MPLS method aims to formulate a multivariate equation in power form as in Eq. (15).

$$y^h = ax_1^{b_1} x_2^{b_2} \dots x_m^{b_m} \quad (15)$$

Least squares procedures shall be carried out as well, yet with different formula of residuals (see Eq. (16)). Therefore, the value of  $a$  and  $b$  in Eq. (15) can be obtained by solving Eq. (17) and the matrix as in Eq. (18).

$$J = \sum_{i=1}^n (\ln(y_i) - \ln(y_i^h))^2 \quad (16)$$

$$a = \exp \left[ \frac{1}{n} \left( \left( \sum_{i=1}^n \ln(y_i) \right) - \sum_{j=1}^m \left( b_j \sum_{i=1}^n \sum_{j=1}^m \ln(x_{j,i}) \right) \right) \right] \quad (17)$$

$$\begin{pmatrix} b_1 \\ b_2 \\ \vdots \\ b_m \end{pmatrix} = \begin{pmatrix} \gamma_1 & -\lambda_{12} & \dots & -\lambda_{1m} \\ -\lambda_{21} & \gamma_2 & \dots & -\lambda_{2m} \\ \vdots & \vdots & \ddots & \vdots \\ -\lambda_{m1} & -\lambda_{m2} & \dots & \gamma_m \end{pmatrix}^{-1} \begin{pmatrix} \xi_1 \\ \xi_2 \\ \vdots \\ \xi_m \end{pmatrix} \quad (18)$$

where

$$\gamma_j = n \left\{ \sum_{i=1}^n \sum_{j=1}^m [\ln(x_{j,i})]^2 \right\} - \left\{ \sum_{i=1}^n \sum_{j=1}^m [\ln(x_{j,i})] \right\}^2 \quad (19)$$

$$\xi_j = n \left[ \sum_{i=1}^n \sum_{j=1}^m \ln(x_{j,i}) \ln(y_j) \right] - \left[ \sum_{i=1}^n \sum_{j=1}^m \ln(x_{j,i}) \right] \left[ \sum_{i=1}^n \ln(y_j) \right] \quad (20)$$

$$\lambda_{j,k} = \left[ \sum_{i=1}^n \sum_{j=1}^m \ln(x_{j,i}) \right] \left[ \sum_{i=1}^n \sum_{j=1}^m \ln(x_{k,i}) \right] - n \left[ \sum_{i=1}^n \sum_{j=1}^m \ln(x_{j,i}) \ln(x_{k,i}) \right] \quad (21)$$

The subscript  $k$  represents the value of second subscript of the term  $\lambda$ . Normalised MPLS equations can be obtained by replacing the value of factors with the normalised value, which can be represented by Eq. (22):

$$\mathbf{X} = C + (\mathbf{x} - \mathbf{x}_{\min}) / (\mathbf{x}_{\max} - \mathbf{x}_{\min}) \quad (22)$$

where  $C$  is the normalising coefficient, which must be a real number. The indices of the normalised MPLS equations could directly indicate the significance level if the coefficient of determination  $R^2$  of the equation exceeds 0.5 [35]. Coefficient of determination  $R^2$  can be defined using Eq. (23):

$$R^2 = \frac{\left( n \sum (yy^h) - \sum (y) \sum (y^h) \right)^2}{\left[ n \left( \sum (y^2) - (\sum y)^2 \right) \right] \left[ n \left( \sum ((y^h)^2) - (\sum (y^h))^2 \right) \right]} \quad (23)$$

The accuracy of the models will be tested too using root mean square error (RMSE), which can be defined as in Eq. (24).

$$\text{RMSE} = \frac{1}{n^2} \sqrt{\sum (y - y^h)^2} \quad (24)$$

### 3 Results and Discussion

The simulation is conducted by setting  $\sigma_s = 200 \times 10^{-6}$  Pa.s,  $\mu = 0.8 \times 10^{-3}$  Pa.s,  $f = 80$  kHz, and  $W = 400$  W as the benchmark sonication parameters. One-factor investigation on the effects of  $\sigma_s$ ,  $\mu$ ,  $f$ , and  $W$  is conducted, within total sonication time of  $2 \times 10^{-7}$  seconds.

#### 3.1 Surface Tension of Biomass-Water

Surface tension  $\sigma_s$  can be defined as the surface energy per unit area, or the Van-der-Waals forces between fluid molecules on the interface. Since the growth and collapse of microbubbles involve complex mechanism of interfacial fluid dynamics, surface tension is one of the major factors dictating the cavitation phenomenon. In bubble dynamics, surface tension administers the maximum pressure difference between inner cavity and outer fluids that the bubble could support.

The history of growth and drop of instantaneous bubble radius due to different surface tension are illustrated as in Fig. 1. The results are computed by setting other variables to be constant, i.e.  $\mu = 0.8 \times 10^{-3}$  Pa.s,  $f = 80$  kHz, and  $W = 400$  W. From Fig. 1, it can be observed that by increasing the surface tension of biomass-water, the intensity of bubble cavitation occurrence will be increased (i.e. 4 cycles for  $\sigma_s = 50 \times 10^{-6}$  Pa.s and 8 cycles for  $\sigma_s = 350 \times 10^{-6}$  Pa.s, within  $2 \times 10^{-7}$  s). Moreover, higher surface tension will result in the formation of larger microbubbles and smaller collapsing radius (see Appendix). The complication of bubble nucleation has increased the pressure difference between the inner and outer part of microbubble, and thus upon its disruption, a higher temperature and pressure hike can be released.  $T_{collapse}$  increases steadily while  $P_{collapse}$ , and  $P_{shock}$  increase in an exponential way with respect to  $\sigma_s$ , which can be illustrated as in Fig. 2. These results are supported by the review works by Thompson and Doraiswamy [37] and Pilli et al. [38] who concluded that by increasing the surface tension, both the cavitation threshold (the maximum bubble radius required before collapsing) and the rate of cavitation will be increased.

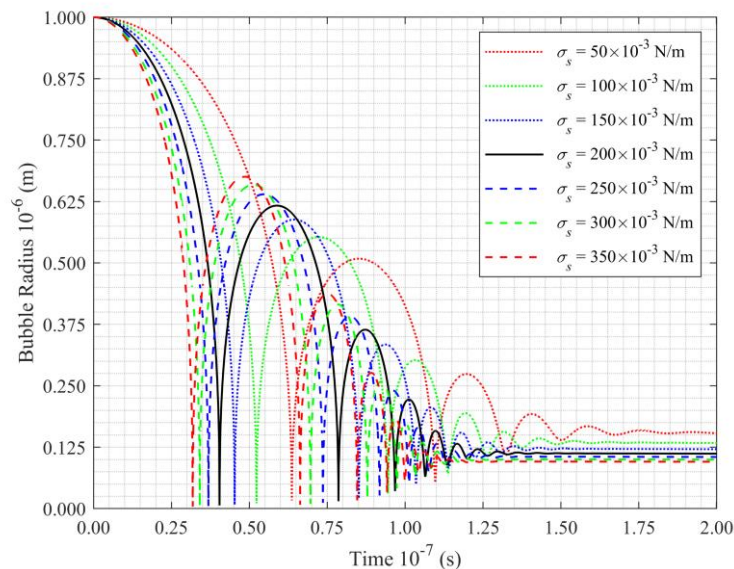


**Fig. 1** Effects of surface tension to the fluctuation of instantaneous bubble radius.

Although higher surface tension could improve the release of mechanical shear to break the ligno-cellulose walls, this does not necessarily improve the pretreatment efficiency. This is because ultrasonic pretreatment is not only determined by intensity of cavitation (bubble disruption), but also the intensity

of bubble formation. The intensity of bubble formation can be represented by the wavelength of capillary wave  $\lambda$ , which is a wave propagating on the fluids' interface where its restoring force is dominated by surface tension. Capillary wave is responsible for the spontaneous rupture of thin liquid film, leading to formation of emulsion and microbubbles [39]. Therefore, the smaller the wavelength of capillary wave, the more intense the formation of microbubble. Unfortunately, RPE is not able to predict the intensity of bubble formation, as the formulation of RPE does not consider surface stress boundary condition. The detailed mathematical description on the interfacial fluid dynamics [40] of capillary wave was recently reported by Shen et al. [41]. The wavelength of capillary wave can be related with the surface tension and sonication frequency [42] via a simple equation as shown in Eq. (25).

$$\lambda = \left( \frac{2\pi\sigma_s}{\rho_\infty f^2} \right)^{1/3} \quad (25)$$

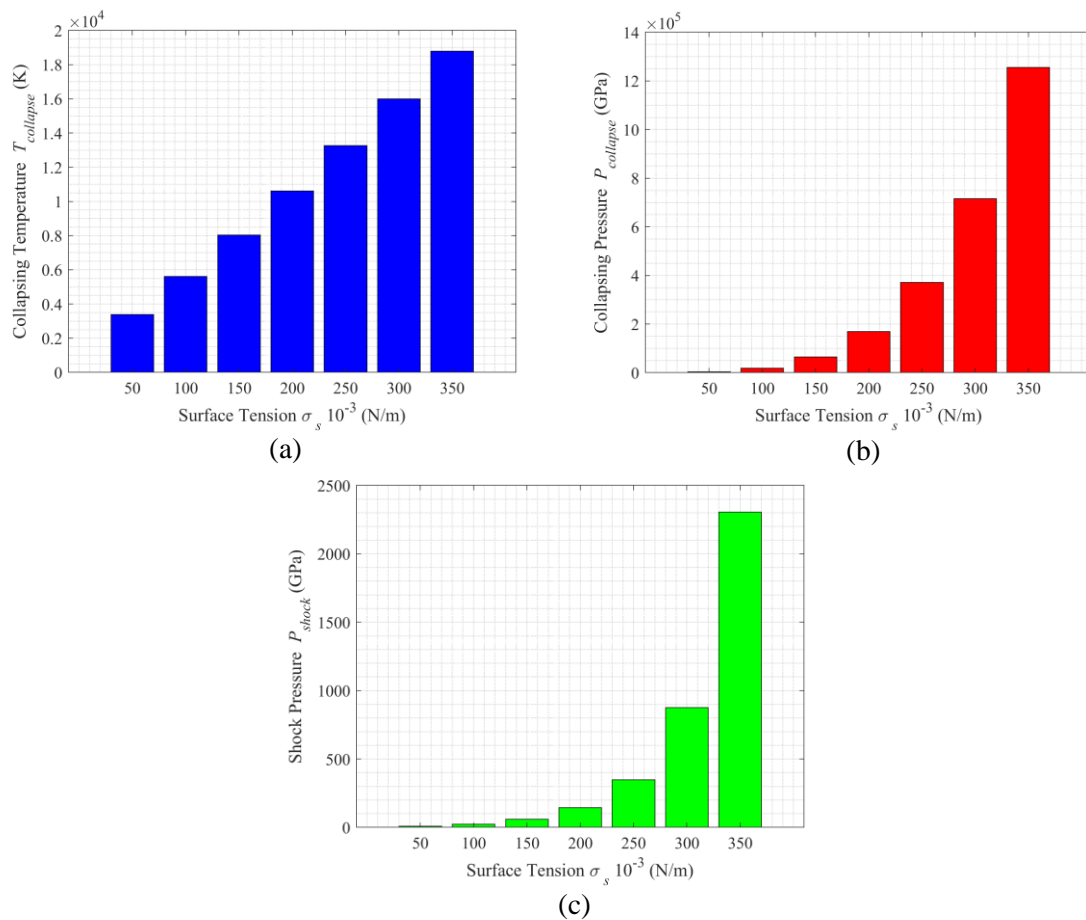


**Fig. 2** Effects of surface tension to (a)  $T_{collapse}$ , (b)  $P_{collapse}$ , and (c)  $P_{shock}$  at  $\mu = 0.8 \times 10^{-3}$  Pa.s,  $f = 80$  kHz, and  $W = 400$  W.

Zhao et al. [43] further explained that fluids with higher surface tension will increase the wavelength of capillary wave and keep the geometry of the bubble to be in spherical shape. This will stabilise the bubble's interface, leading to a higher cavitation threshold. Inclusion of surfactant will induce rheological response and reduce surface tension [44], and therefore it will facilitate the breakup event of thin fluid film and formation of microbubbles.

Camerotto et al. [45] discovered that low surface tension fluid will render a higher acoustical noise and better ultrasonic cleansing effect. The experiment conducted by Lee et al. [46] recently also illustrated that by decreasing the surface tension, the efficiency of ultrasonic pretreatment on biomass

compound is improved. Hence, it can be concluded that in determining the pretreatment efficiency, the intensity of formation of microbubbles is more dominant than the unleashing of mechanical shear.

### 3.2 Dynamic Viscosity of Biomass-Water

Dynamic viscosity  $\mu$  (named as viscosity thereafter) is ratio between wall shear stress and shear rate, which also represents the internal flow friction. In this simulation, Newtonian fluid is assumed such that viscosity does not change with shear rate. From our previous derivation work [22], it can be inferred that viscosity is the factor which determines the resistance for the expansion or contraction of microbubbles. In other words, theoretically, biomass-fluid with higher viscosity tends to restrict the growing or collapsing of microbubbles.

The bubble radius due to different viscosity can be shown as in Fig. 3. The other factors are set constant such that  $\sigma_s = 200 \times 10^{-3}$  N/m,  $f = 80$  kHz, and  $W = 400$  W. It can be clearly observed that in Fig. 3 and Appendix, biomass-water with lower viscosity would be able to generate microbubbles with larger radius ratio ( $R_{max}/R_{min}$ ) because of low internal resistance. This implies that a more powerful shockwave could be emitted. From Fig. 4, it can be observed that high viscosity generally reduces all the  $T_{collapse}$ ,  $P_{collapse}$ , and  $P_{shock}$ . It is also noteworthy that at low viscosity as well, the coalescence mechanism [47] does not decay easily, and the microbubbles tend to continue to collapse and rebound. Therefore, for a case with similar intensity of bubble generation (i.e. same value of  $\sigma_s$ ,  $\rho_\infty$ , and  $f$ ), biomass-water with low viscosity possesses excellent advantage in improving the ultrasonic cavitation.

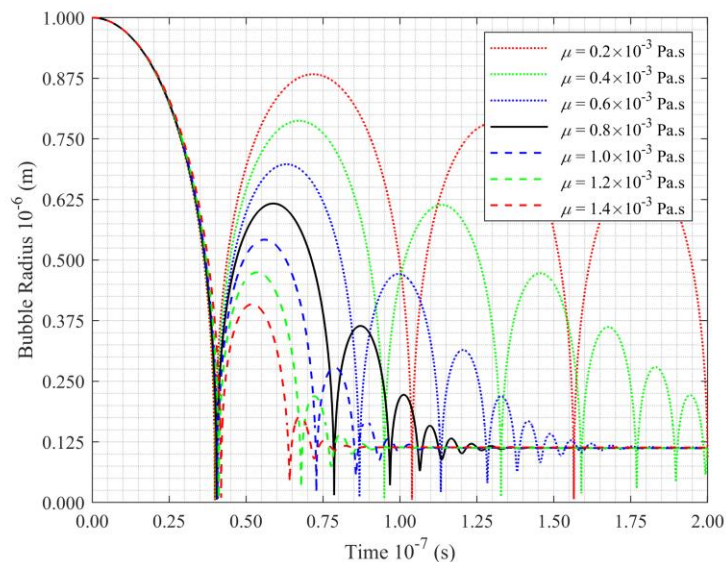


**Fig. 3** Effects of dynamic viscosity to the fluctuation of instantaneous bubble radius.

Other significance of viscosity is its role in the generation of acoustic streaming, which can be regarded as the sound wave attenuation in acoustic propagation. This is related to the acoustical behaviour of the fluid, in which drag force on the expansion of bubble is generated as a result of sound energy absorption ability of the fluids. The absorption capability can be further measured using acoustic attenuation coefficient  $\beta$ , which can be physically defined as the ratio between the absorbed sound energy and total sound energy from a medium. According to Lighthill [48], acoustic attenuation coefficient  $\beta$  is closely related with fluid's Reynold's stress [49], and therefore it is directly proportional with viscosity as shown in Eq. (26).

$$\beta = \left( \frac{2\pi f}{c^{3/2}} \right)^2 \left( \frac{4\mu}{3\rho_\infty} \right) \quad (26)$$

The detailed description for the physics of acoustic streaming can be found in the work of Tang et al. [50] and Yasui [11]. Although there are different types of acoustic streaming, Eckart streaming is the sound dissipating mechanism directly induced by viscosity. In Eckart streaming, the energy



attenuation is provoked by the effect of bulk viscosity or volume viscosity which is an irreversible resistance due to molecular vibration and sound-wave-generated vorticity. The mathematical formulation for such streaming can be referred in the seminal work reported by Eckart [51], meanwhile the power loss due to the streaming was further discussed by Sojahrood et al. [52]. With this regard, the attenuation effect shall be included in the investigation, and Eq. (6), (7), and (8) shall be recalculated using Eq. (27), (28), and (29) respectively. With these attenuations,  $T_{collapse}$ ,  $P_{collapse}$ , and  $P_{shock}$  is further tempered in all range of dynamic viscosity which can be seen in Fig. 4.

$$T_{collapse} = (1 - \beta) T_{\infty} \left( \frac{R_{max}}{R} \right)^{3(\eta-1)} \quad (27)$$

$$P_{collapse} = (1 - \beta) \left[ P_v + P_g \left( \frac{R_0}{R_{max}} \right)^3 \right] \left( \frac{R_{max}}{R} \right)^{3\eta} \quad (28)$$

$$P_{shock} = (1 - \beta) c_1 \rho_{\infty} u_s \left[ 10^{(u_s - c)/c_2} - 1 \right] + P_{\infty} \quad (29)$$

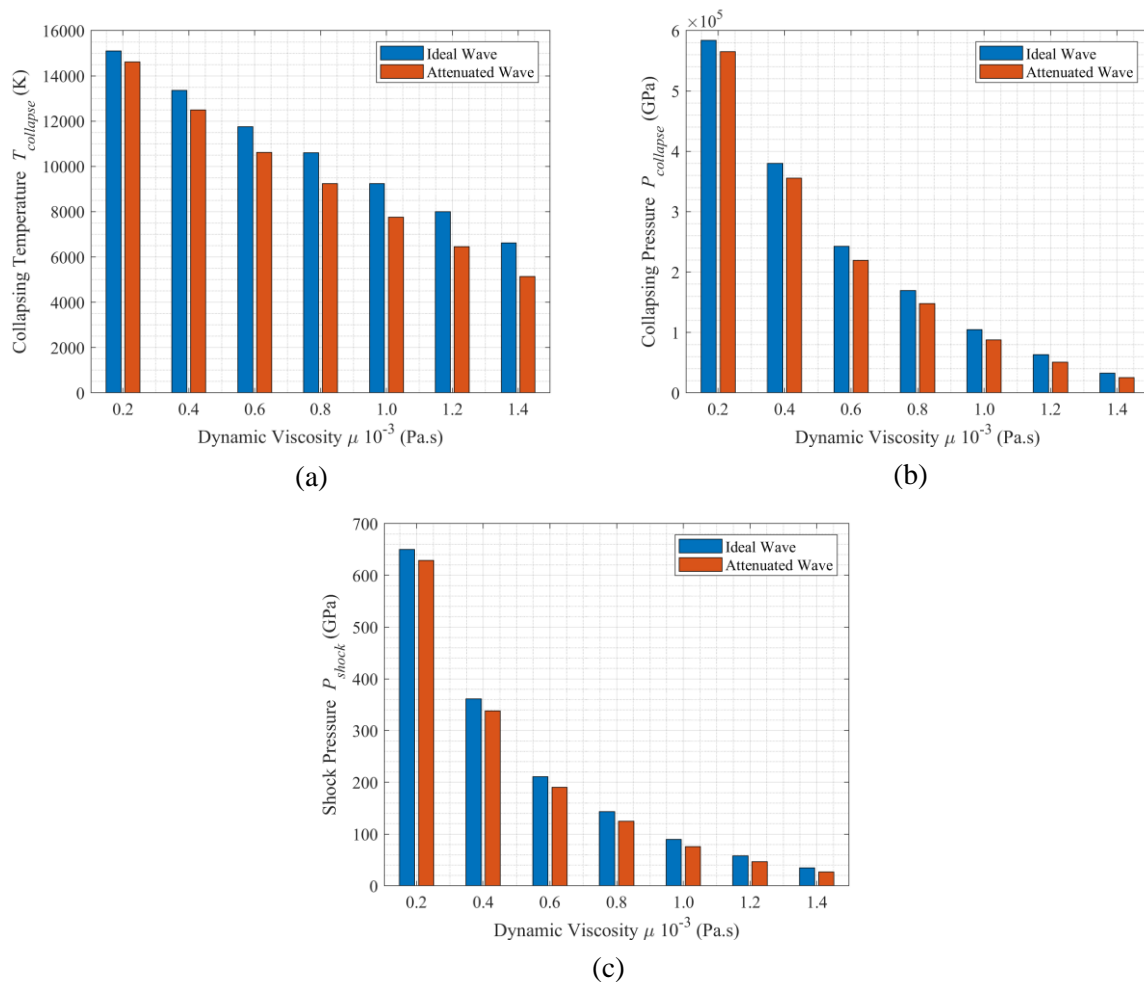


**Fig. 4** Effects of dynamic viscosity  $\mu$  to (a)  $T_{collapse}$ , (b)  $P_{collapse}$ , and (c)  $P_{shock}$  at  $\sigma_s = 200 \times 10^{-3}$  N/m,  $f = 80$  kHz, and  $W = 400$  W.

The computational results in current work (see Fig. 3 and Fig. 4) are in good agreement with the work reported by Zhang et al. [53] who concluded that low viscosity would lead to lower damping on shockwave, higher cavitation speed, and continuous occurrence of cavitation. An experiment conducted by Dewil et al. [54] reported the observation that at high viscosity, more acoustical energy was absorbed

to transform into thermal energy instead of cavitation energy. Moreover, Helfield et al. [55] found that higher viscosity could reduce the propensity of microbubbles' fragmentation, while the experiment by Tzanakis et al. [56] also observed a stronger signal of acoustic attenuation for high viscosity fluids. Hence, in general, a biomass-water with lower viscosity is more favourable in ultrasonic cavitation.

### 3.3 Sonication Frequency

The variation of sonication frequency  $f$  does not affect much on the decaying tendency of coalescence mechanism under constant surface tension and dynamic viscosity as demonstrated in Fig. 5. The current simulation revealed that the increment of frequency will slightly increase the radius ratio, which signifies a marginal enhancement of collapsing energy. Nonetheless, the increment of frequency will greatly attenuate the ultrasonic energy with the correlation of  $\beta \propto f^2$  as shown in Eq. (25), and this has been discussed too in detail by Muthukumaran et al. [57]. The difference between the ideal and attenuated sonication effects can be referred as in Fig. 6. Such an acoustic streaming will result in a noticeable declining trend in all collapsing temperature and pressure (see Table 2). There is a slight increase in shock pressure between 20 kHz and 60 kHz, yet it drops apparently after 60 kHz. However, the increase of frequency will shorten the capillary wavelength and form more microbubbles (see Eq. (25)).

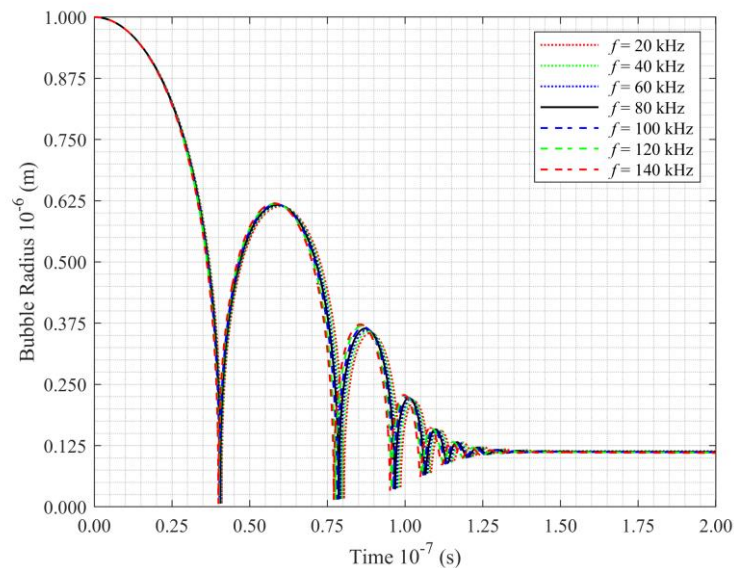


**Fig. 5** Effects of sonication frequency to the fluctuation of instantaneous bubble radius.

Although current simulation shows that the shearing effect of microjet is reduced at higher frequency due to attenuation, there is so far no conclusive relationship between frequency and ultrasonic pretreatment. A discussion by Crum [58] commented that low frequency ultrasound provides more time for the bubble to grow, and therefore will lead to a more violent collapse of bubble, emitting a stronger shock wave to the surrounding. However, Crum [58] deduced that low frequency would reduce the rate of bubble formation, which is in accordance with the theory of capillary wave. The continual cavitation activities during high frequency would produce more free radicals [58], which could be beneficial for ultrasonic cavitation. In other words, low frequency would favour the mechanical shearing while high frequency will induce more sonochemical reactions. The idea is then widely subscribed by many researchers later, which can be evidenced in the work of Zhang et al. [59], Pilli et al. [38], Ashokkumar [60], Iskalieva et al. [61], and Luo et al. [62]. Experiments conducted by Tiehm et al. [63] and Zhang et al. [59] also proved that low frequency sonication could improve the disintegration of sludge. Nonetheless, the analysis by Vichare et al. [64], optimisation of transesterification of soybean oil by Mahamuni and Adewuyi [65], and the experiment of ultrasonic pretreatment soft wood biomass by Cherpozat et al. [66] showed the opposite trend that the high frequency sonication will improve these pretreatment efficiency. Review works by Luo et al. [62] further confirmed that high frequency ultrasound favours the decomposition of biomass mixtures such as hydrous bioethanol, solid sucrosecorn oil suspension, and microcrystalline cellulose.

Therefore, the selection of operating frequency shall be relied on the intended physical or chemical reaction and biomass compound, i.e. whether the disruption of compounds require more on mechanical shear or free radical reaction [1]. Le et al. [67] emphasized that the selection of optimal ultrasonic frequency is dependent on the expected ultrasonic effects. Similarity discourse on the issue can be found too in the work by Sivaramakrishnan and Incharoensakdi [68]. This is further supported by the experiment by Kurokawa et al. [69] who showed that the pretreatment efficiency is more dependent on the species and structure of microalgae instead of sonication frequency. A recent review by Nagarajan et al. [70] have listed down the optimal frequency for different types of algae. Since the effect of sonication frequency to biomass pretreatment is so far not yet resolved, there are still great room for detailed investigation, including the application of frequency within the audible range [67].

In current simulation, the low frequency sonication would generally release higher collapsing pressure and temperature, yet with the expense of the intensity bubble formation. In the contrast, at high ultrasonic frequency, great sound energy attenuation could be observed (as in Fig. 6) although more microbubbles could be formed. The divergence of conclusion in experimental reports revealed that it is incorrect to directly conclude how the frequency could directly affect sonication efficiency, as the efficiency is also greatly dependent on the biomass process and species.

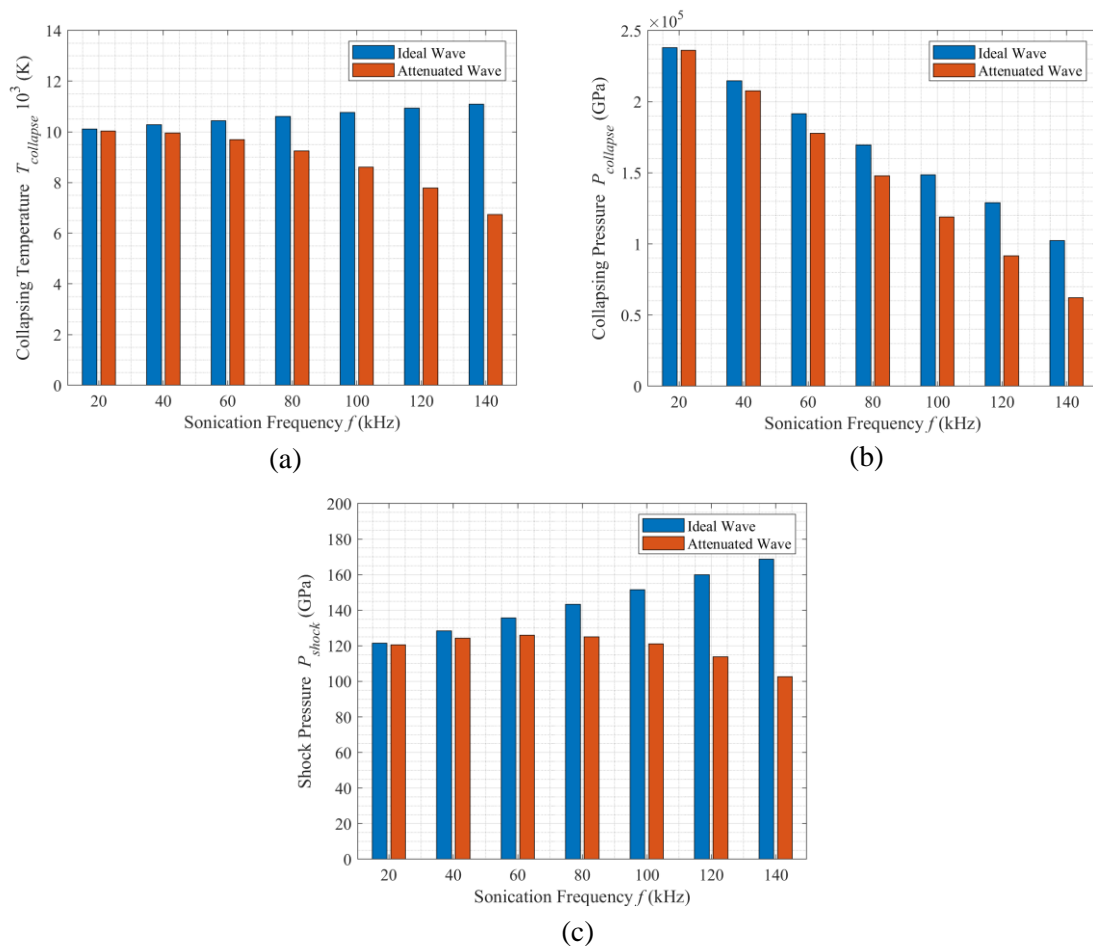


**Fig. 6** Effects of frequency  $f$  to (a)  $T_{collapse}$ , (b)  $P_{collapse}$ , and (c)  $P_{shock}$  at  $\sigma_s = 200 \times 10^{-6}$  Pa.s,  $\mu = 0.8 \times 10^{-3}$  Pa.s, and  $W = 400$  W.

### 3.4 Sonication Power

Sonication power  $W$  will not influence much on the fluctuation pattern of microbubbles as shown in Fig. 7. However, modelling on RPE revealed that increasing the sonication power would have positive physical effect on the sonication performance (i.e. increasing collapsing temperature, collapsing pressure, and shock pressure) as in Fig. 8. The observation is in good agreement with the discussion reported

by Karimi et al. [1], Muthukumaran et al. [57], and Zhang et al. [59], such that higher power would have better sonication efficiency. Pilli et al. [37] commented that the increment of sonication power can compensate the energy attenuation due to acoustic streaming, especially under operating conditions of high frequency and high viscosity.

Nonetheless, most of the reports [1,57,59] stressed that while the sonication efficiency is enhanced due to an increased sonication power, an optimal power will be reached, and upon the optimal power, the sonication performance will drop. This is because higher power would form greater bubble radius, then therefore a bubble cluster will be formed which would hinder the transmission of acoustic energy. Mahamuni and Adewuyi [65] conducted optimisation experiment on the transesterification of soybean oil and they also observed that a higher sonication power would improve the efficiency of formation of biodiesel, yet with a possible existence of optimal power. An optimisation on ultrasonic power consumption is therefore required for a more practical up-scale industrial application.

Perhaps, the current simulation is limited to single bubble cavitation, in which the possible formation of bubble cluster is impossible to be observed under current mathematical model. Chong et al. [71] proposed a coupling of oscillator approximation into Keller-Miksis equation to predict the radius growth of microbubble within a small bubble cluster. A more advanced simulation using fundamental partial differential equations in Computational Fluid Dynamics [47] is required to study how the bubble cluster can be formed and how the cluster could hinder the propagation of acoustical vibration.

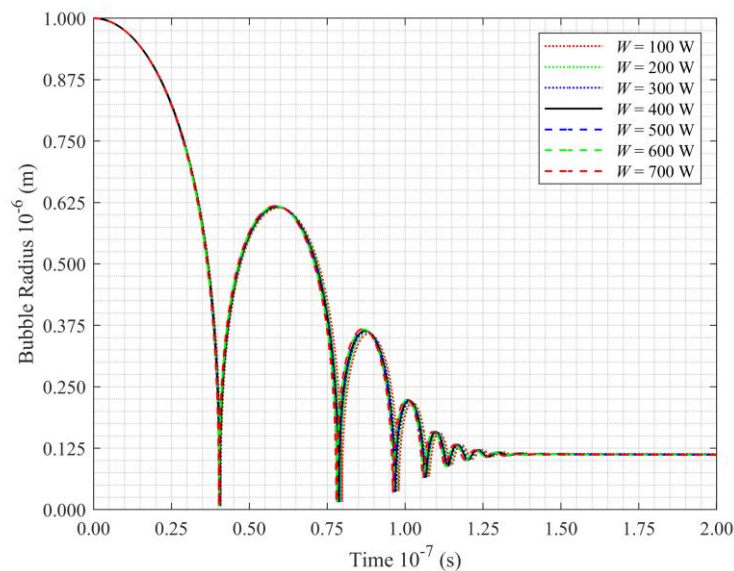


**Fig. 7** Effects of sonication power to the fluctuation of instantaneous bubble radius.

### 3.5 Multivariate Analysis on Sonication Parameters

The relationship between  $\sigma_s$ ,  $\mu$ ,  $f$ , and  $W$  with  $T_{collapse}$ ,  $P_{collapse}$ , and  $P_{shock}$  is investigated too using MLS and normalised MPLS method. The MLS and normalised MPLS equations for the multivariate study can be obtained from Eqs. (30) to (35). The normalising coefficient  $C$  of 0.2 is applied as it would provide the best fitted MPLS equations.

**MLS equations:**

$$T_{collapse}^h = 8.1568 \times 10^3 + 3.9903 \times 10^4 \sigma_s - 1.0240 \times 10^4 \mu + 10.8420 f + 1.1629 W \\ + 1.4077 \times 10^4 \sigma_s^2 + 1.5752 \times 10^3 \mu^2 - 0.2384 f^2 - 4.9690 \times 10^4 W^2 \quad (30)$$

$$P_{collapse}^h = 1.2333 \times 10^6 - 6.7994 \times 10^6 \sigma_s - 1.0194 \times 10^6 \mu - 1.5470 \times 10^3 f + 60.6924 W \\ + 2.3699 \times 10^7 \sigma_s^2 + 3.7669 \times 10^5 \mu^2 + 0.5964 f^2 - 0.0229 W^2 \quad (31)$$

$$P_{shock}^h = 3.2870 \times 10^3 - 2.6645 \times 10^4 \sigma_s - 1.2431 \times 10^3 \mu + 0.3777 f - 0.0362 W \\ + 7.0353 \times 10^4 \sigma_s^2 + 503.1594 \mu^2 - 0.0032 f^2 + 1.7268 \times 10^{-7} W^2 \quad (32)$$

MPLS equations:

$$T_{collapse}^h = 9.6531 \times 10^3 \sigma_s^{0.9376} \mu^{-0.5272} f^{-0.1802} W^{0.0105} \quad (33)$$

$$P_{collapse}^h = 1.9859 \times 10^5 \sigma_s^{3.2965} \mu^{-1.5483} f^{-0.6561} W^{0.0519} \quad (34)$$

$$P_{shock}^h = 214.7172 \sigma_s^{2.9301} \mu^{-1.5933} f^{-0.0264} W^{0.1120} \quad (35)$$

The value of  $R^2$  and accumulative errors from Eq. (30) to Eq. (35) can be listed as in Table 2. From Table 2, MLS equations fit the sonication parameters better, and this implies that most of the sonication phenomenon is optimisable. MPLS method fits well only for collapsing temperature.  $R^2$  for MPLS equations are generally low, and this can be attributed to the fact the current simulation does not involve any interaction study among the sonication parameters. It shall be noted that MPLS equations signify the close interaction between the factors.

Although the  $R^2$  for other MPLS equations is low, the consistent ranking of the magnitude of indexes of all the MPLS models lead to similar conclusion. It can be inferred from MPLS equations that, for all  $T_{collapse}$ ,  $P_{collapse}$ , and  $P_{shock}$ , surface tension has the highest positive significance on the sonication performance, followed by power. Meanwhile, viscosity possesses the strongest negative significance, followed by frequency. In short, the fluid properties of biomass-water generally play a more critical role than sonication frequency and power.

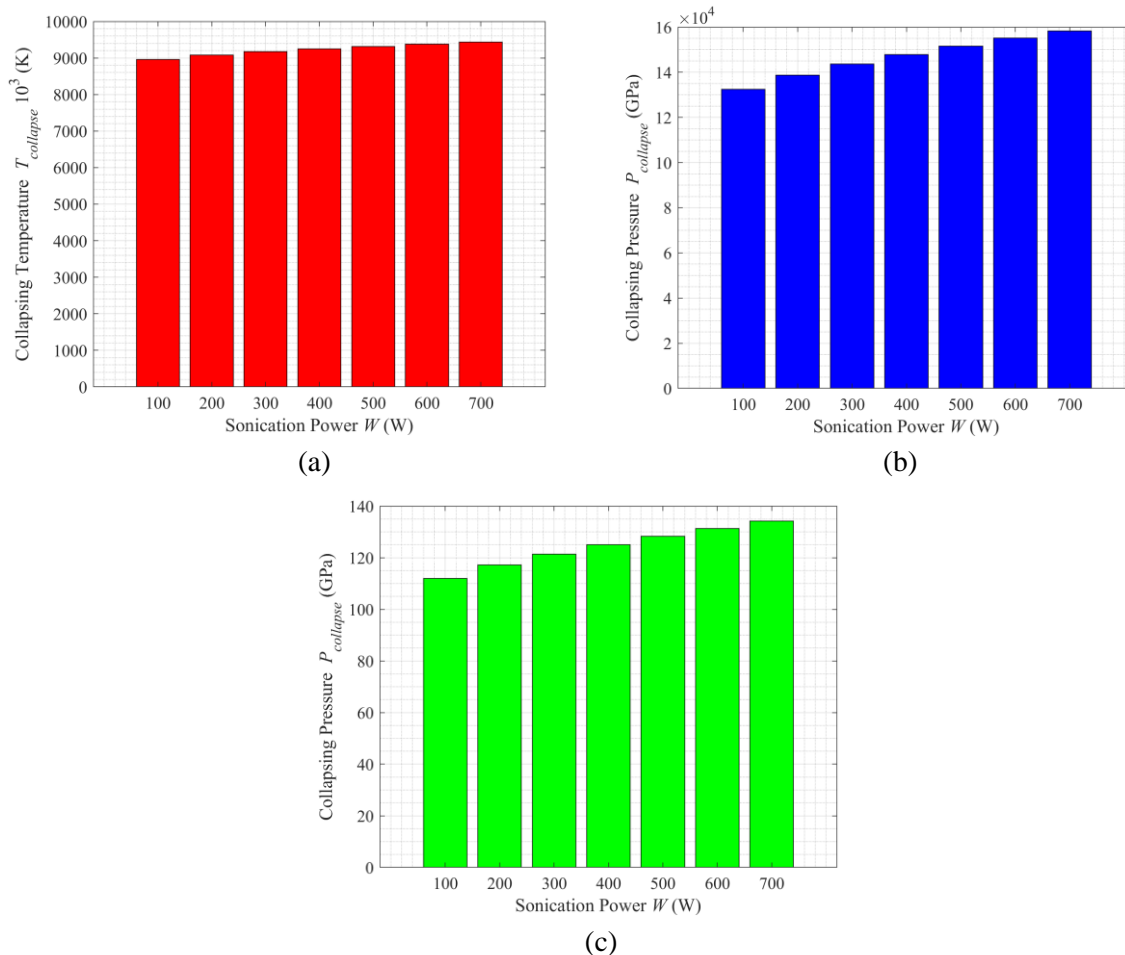


**Fig. 8** Effects of power  $W$  to (a)  $T_{collapse}$ , (b)  $P_{collapse}$ , and (c)  $P_{shock}$  at  $\sigma_s = 200 \times 10^{-6}$  Pa.s,  $\mu = 0.8 \times 10^{-3}$  Pa.s, and  $f = 80$  kHz.

**Table 2** Value of  $R^2$  and accumulative errors for the approximated equations.

Equation	$R^2$	RMSE
(30)	0.9994	72.5224
(31)	0.9393	56757.4195
(32)	0.5581	310.7019
(33)	0.9239	806.7833
(34)	0.2656	359840.6413
(35)	0.1296	412.0277

## 4 Conclusion

Computational modelling based on RPE for the effects of  $\sigma_s$ ,  $\mu$ ,  $f$ , and  $W$  on sonication performance such as  $T_{collapse}$ ,  $P_{collapse}$ , and  $P_{shock}$  has been conducted, and the computational results revealed that:

1. Increasing  $\sigma_s$  will enhance the sonication energy, yet with the expense of limiting the formation of bubble, which would eventually deteriorate the sonication performance.
2. Increasing  $\mu$  will suppress the growth of bubble and promote larger acoustic streaming, leading to an overall drop of sonication performance.
3. Increasing  $f$  might slightly enhance the bubble growth, yet it will greatly be attenuated, and this results in a low sonication performance at high  $f$ . However, the application of  $f$  shall depend on the species of biomass to be pre-treated, as high  $f$  would promote the active release of free radicals.
4. Increasing  $W$  would be beneficial for sonication effects, yet with a possible optimal power to avoid the formation of bubble cluster which will set back the ultrasound propagation.

Perhaps, current simulation is limited only to one-factor investigation, in which the interactions between the sonication parameters does not take into consideration. Moreover, RPE models are limited only for incompressible cavitation, and there are many factors being neglected in the current model such as the supersonic bubble growth, formation of bubble cluster, and attenuation of sonication energy due to bulk modulus. Interfacial fluid dynamics are required for a detailed investigation for the complicated physics of bubble dynamics under ultrasonic pretreatment. Despite the current work has successfully demonstrated the effects of these sonication parameters, more research is required in the near future.

## Declaration of Conflict of Interest

The authors declared that there is no conflict of interest with any other party on the publication of the current work.

## ORCID

Wah Yen Tey  <https://orcid.org/0000-0002-1865-9212>

Kiat Moon Lee  <https://orcid.org/0000-0003-1126-9657>

## References

- [1] M. Karimi, B. Jenkins, P. Stroeve, Ultrasound irradiation in the production of ethanol from biomass, *Renewable and Sustainable Energy Reviews*. 40 (2014) 400–421. <https://doi.org/10.1016/j.rser.2014.07.151>.
- [2] I. John, J. Pola, A. Appusamy, Optimization of Ultrasonic Assisted Saccharification of Sweet Lime Peel for Bioethanol Production Using Box–Behnken Method, *Waste and Biomass Valorization*. 10 (2019) 441–453. <https://doi.org/10.1007/s12649-017-0072-1>.
- [3] J.D. Quek, K.M. Lee, S. Lim, W.Y. Tey, H.-S. Kang, L.K. Quen, Delignification of oil palm empty fruit bunch via ultrasound-assisted deep eutectic solvent pretreatment, *IOP Conference Series: Earth and Environmental Science*. 463 (2020) Article ID 012007. <https://doi.org/10.1088/1755-1315/463/1/012007>.
- [4] K.M. Lee, M.F. Zani, K.K. Chan, Z.P. Chin, Y.C. Liu, S. Lim, Synergistic ultrasound-assisted organosolv pretreatment of oil palm empty fruit bunches for enhanced enzymatic saccharification: An optimization study using artificial neural networks, *Biomass and Bioenergy*. 139 (2020) Article ID 105621. <https://doi.org/10.1016/j.biombioe.2020.105621>.

- [5] K.S. Suslick, Sonochemistry, *Science*. 247 (1990) 1439–1445. <https://doi.org/10.1126/science.247.4949.1439>.
- [6] W. Gpel, K.D. Schierbaum, C.G. Vayenas, I. v. Yentekakis, H. Gerischer, W. Vielstich, P.E. Savage, R.B. Moyes, G. Bond, K.S. Suslick, Special Catalytic Systems, in: *Handbook of Heterogeneous Catalysis*, Wiley-VCH Verlag GmbH, Weinheim, Germany, 1997. <https://doi.org/10.1002/9783527619474.ch8>.
- [7] M. Kunaver, E. Jasiukaitytė, N. Čuk, Ultrasonically assisted liquefaction of lignocellulosic materials, *Bioresource Technology*. 103 (2012) 360–366. <https://doi.org/10.1016/j.biortech.2011.09.051>.
- [8] A. Ranjan, C. Patil, V.S. Moholkar, Mechanistic Assessment of Microalgal Lipid Extraction, *Industrial & Engineering Chemistry Research*. 49 (2010) 2979–2985. <https://doi.org/10.1021/ie9016557>.
- [9] C.E. Brennen, Bubble Growth and Collapse, in: *Fundamentals of Multiphase Flow*, Cambridge University Press, 2014: pp. 100–127. <https://doi.org/10.1017/cbo9780511807169.005>.
- [10] S. Merouani, O. Hamdaoui, Y. Rezgui, M. Guemini, Mechanism of the sonochemical production of hydrogen, *International Journal of Hydrogen Energy*. 40 (2015) 4056–4064. <https://doi.org/10.1016/j.ijhydene.2015.01.150>.
- [11] K. Yasui, Bubble Dynamics, in: *Acoustic Cavitation and Bubble Dynamics: Theoretical and Computational Chemistry*, 2018: pp. 37–97. [https://doi.org/10.1007/978-3-319-68237-2\\_2](https://doi.org/10.1007/978-3-319-68237-2_2).
- [12] C.-Y. Yang, T.J. Fang, Combination of ultrasonic irradiation with ionic liquid pretreatment for enzymatic hydrolysis of rice straw, *Bioresource Technology*. 164 (2014) 198–202. <https://doi.org/10.1016/j.biortech.2014.05.004>.
- [13] H. Wu, X. Dai, S.-L. Zhou, Y.-Y. Gan, Z.-Y. Xiong, Y.-H. Qin, J. Ma, L. Yang, Z.-K. Wu, T.-L. Wang, W.-G. Wang, C.-W. Wang, Ultrasound-assisted alkaline pretreatment for enhancing the enzymatic hydrolysis of rice straw by using the heat energy dissipated from ultrasonication, *Bioresource Technology*. 241 (2017) 70–74. <https://doi.org/10.1016/j.biortech.2017.05.090>.
- [14] G.D. Saratale, R.G. Saratale, S. Varjani, S.-K. Cho, G.S. Ghodake, A. Kadam, S.I. Mulla, R.N. Bharagava, D.-S. Kim, H.S. Shin, Development of ultrasound aided chemical pretreatment methods to enrich saccharification of wheat waste biomass for polyhydroxybutyrate production and its characterization, *Industrial Crops and Products*. 150 (2020) Article ID 112425. <https://doi.org/10.1016/j.indcrop.2020.112425>.
- [15] K.M. Lee, K.N. Ng, Effect of ultrasonication in Organosolv pretreatment for enhancement of fermentable sugars recovery from palm oil empty fruit bunches, *Progress in Energy and Environment*. 11 (2019) 15–23. <http://www.akademiabaru.com/submit/index.php/progee/article/view/1059>.
- [16] K. Ninomiya, K. Kamide, K. Takahashi, N. Shimizu, Enhanced enzymatic saccharification of kenaf powder after ultrasonic pretreatment in ionic liquids at room temperature, *Bioresource Technology*. 103 (2012) 259–265. <https://doi.org/10.1016/j.biortech.2011.10.019>.
- [17] A.I. Khuri, S. Mukhopadhyay, Response surface methodology, *Wiley Interdisciplinary Reviews: Computational Statistics*. 2 (2010) 128–149. <https://doi.org/10.1002/wics.73>.
- [18] O.A. Fakayode, E.A.A. Aboagrib, D. Yan, M. Li, H. Wahia, A.T. Mustapha, C. Zhou, H. Ma, Novel two-pot approach ultrasonication and deep eutectic solvent pretreatments for watermelon rind delignification: Parametric screening and optimization via response surface methodology, *Energy*. 203 (2020) Article ID 117872. <https://doi.org/10.1016/j.energy.2020.117872>.
- [19] S. Merouani, O. Hamdaoui, Y. Rezgui, M. Guemini, Effects of ultrasound frequency and acoustic amplitude on the size of sonochemically active bubbles-Theoretical study, *Ultrasonics Sonochemistry*. 20 (2013) 815–819. <https://doi.org/10.1016/j.ultsonch.2012.10.015>.
- [20] B. Sajjadi, P. Asaithambi, A.R. Abdul Aziz, S. Ibrahim, Mathematical analysis of the effects of operating conditions and rheological behaviour of reaction medium on biodiesel synthesis under ultrasound irradiation, *Fuel*. 184 (2016) 637–647. <https://doi.org/10.1016/j.fuel.2016.06.120>.
- [21] J.H. Lee, W.Y. Tey, K.M. Lee, H.-S. Kang, K.Q. Lee, Numerical simulation on ultrasonic cavitation due to superposition of acoustic waves, *Materials Science for Energy Technologies*. 3 (2020) 593–600. <https://doi.org/10.1016/j.mset.2020.06.004>.
- [22] W.Y. Tey, H. Alehossein, Z. Qin, K.M. Lee, H.S. Kang, K.Q. Lee, On stability of time marching in numerical solutions of rayleigh-plesset equation for ultrasonic cavitation, *IOP Conference Series: Earth and Environmental Science*. 463 (2020) Article ID 012117. <https://doi.org/10.1088/1755-1315/463/1/012117>.
- [23] W.Y. Tey, K.M. Lee, C.S. Nor Azwadi, A. Yutaka, Delfim-Soares explicit time marching method for modelling of ultrasonic wave in microalgae pre-treatment, *IOP Conference Series: Earth and Environmental Science*. 268 (2019) Article ID 012106. <https://doi.org/10.1088/1755-1315/268/1/012106>.
- [24] S.C. Chapra, R.P. Canale, Runge-Kutta Methods, in: *Numerical Methods for Engineers*, 6th ed., McGraw Hill Higher Education, 2010: pp. 707–751.
- [25] S. Merouani, O. Hamdaoui, Y. Rezgui, M. Guemini, Energy analysis during acoustic bubble oscillations: Relationship between bubble energy and sonochemical parameters, *Ultrasonics*. 54 (2014) 227–232. <https://doi.org/10.1016/j.ultras.2013.04.014>.
- [26] E.A. Brujan, T. Ikeda, Y. Matsumoto, On the pressure of cavitation bubbles, *Experimental Thermal and Fluid Science*. 32 (2008) 1188–1191. <https://doi.org/10.1016/j.expthermflusci.2008.01.006>.
- [27] M.H. Rice, J.M. Walsh, Equation of State of Water to 250 Kilobars, *The Journal of Chemical Physics*. 26 (1957) 824–830. <https://doi.org/10.1063/1.1743415>.

- [28] S. Merouani, O. Hamdaoui, Y. Rezgou, M. Guemini, Computational engineering study of hydrogen production via ultrasonic cavitation in water, *International Journal of Hydrogen Energy*. 41 (2016) 832–844. <https://doi.org/10.1016/j.ijhydene.2015.11.058>.
- [29] P. Lancaster, K. Salkauskas, Surfaces generated by moving least squares methods, *Mathematics of Computation*. 37 (1981) 141–158. <https://doi.org/10.1090/S0025-5718-1981-0616367-1>.
- [30] P. Breitkopf, A. Rassineux, P. Villon, An Introduction to Moving Least Squares Meshfree Methods, *Revue Européenne Des Éléments Finis*. 11 (2002) 825–867. <https://doi.org/10.3166/reef.11.825-867>.
- [31] K.M. Liew, C. Feng, Y. Cheng, S. Kitipornchai, Complex variable moving least-squares method: A meshless approximation technique, *International Journal for Numerical Methods in Engineering*. 70 (2007) 46–70. <https://doi.org/10.1002/nme.1870>.
- [32] G.R. Joldes, H.A. Chowdhury, A. Wittek, B. Doyle, K. Miller, Modified moving least squares with polynomial bases for scattered data approximation, *Applied Mathematics and Computation*. 266 (2015) 893–902. <https://doi.org/10.1016/j.amc.2015.05.150>.
- [33] S. Zheng, R. Feng, A. Huang, A modified moving least-squares suitable for scattered data fitting with outliers, *Journal of Computational and Applied Mathematics*. 370 (2020) Article ID 112655. <https://doi.org/10.1016/j.cam.2019.112655>.
- [34] G.R. Liu, Y.T. Gu, Meshfree Shape Function Construction, in: *An Introduction to Meshfree Methods and Their Programming*, Springer, Singapore, AA Dordrecht, The Netherlands, 2005: pp. 54–114.
- [35] W.Y. Tey, K.M. Lee, Y. Asako, L.K. Tan, N. Arai, Multivariable power least squares method: Complementary tool for Response Surface Methodology, *Ain Shams Engineering Journal*. 11 (2020) 161–169. <https://doi.org/10.1016/j.asej.2019.08.002>.
- [36] W.Y. Tey, N.A.C.S. Sidik, A. Yutaka, Mohammed W. Muhieldeen, A. Omid, Moving least squares method and its improvement: A concise review, *Journal of Applied and Computational Mechanics*. (2021) 1–7. <https://doi.org/10.22055/JACM.2021.35435.2652>.
- [37] L.H. Thompson, L.K. Doraiswamy, Sonochemistry: Science and Engineering, *Industrial & Engineering Chemistry Research*. 38 (1999) 1215–1249. <https://doi.org/10.1021/ie9804172>.
- [38] S. Pilli, S. Yan, P. Bhunia, R.D. Tyagi, R.Y. Surampalli, R.J. LeBlanc, Ultrasonic pretreatment of sludge: A review, *Ultrasonics Sonochemistry*. 18 (2010) 1–18. <https://doi.org/10.1016/j.ultsonch.2010.02.014>.
- [39] F. Blanchette, T.P. Bigioni, Partial coalescence of drops at liquid interfaces, *Nature Physics*. 2 (2006) 254–257. <https://doi.org/10.1038/nphys268>.
- [40] V.G. Levich, V.S. Krylov, Surface-Tension-Driven Phenomena, *Annual Review of Fluid Mechanics*. 1 (1969) 293–316. <https://doi.org/10.1146/annurev.fl.01.010169.001453>.
- [41] L. Shen, F. Denner, N. Morgan, B. van Wachem, D. Dini, Capillary waves with surface viscosity, *Journal of Fluid Mechanics*. 847 (2018) 644–663. <https://doi.org/10.1017/jfm.2018.364>.
- [42] Z. Dong, C. Yao, Y. Zhang, G. Chen, Q. Yuan, J. Xu, Hydrodynamics and mass transfer of oscillating gas-liquid flow in ultrasonic microreactors, *AIChE Journal*. 62 (2016) 1294–1307. <https://doi.org/10.1002/aic.15091>.
- [43] S. Zhao, C. Yao, Q. Zhang, G. Chen, Q. Yuan, Acoustic cavitation and ultrasound-assisted nitration process in ultrasonic microreactors: The effects of channel dimension, solvent properties and temperature, *Chemical Engineering Journal*. 374 (2019) 68–78. <https://doi.org/10.1016/j.cej.2019.05.157>.
- [44] M. Bruce R., Y. Donald F., O. Theodore H., *Fundamentals of Fluid Mechanics*, Fifth, John Wiley & Sons (Asia) Pte Ltd, Singapore, 2006.
- [45] E. Camerotto, S. Brems, M. Hauptmann, A. Pacco, H. Struyf, P.W. Mertens, S. de Gendt, Influence of surface tension on cavitation noise spectra and particle removal efficiency in high frequency ultrasound fields, *Journal of Applied Physics*. 112 (2012) Article ID 114322. <https://doi.org/10.1063/1.4768472>.
- [46] K.M. Lee, J.Y. Hong, W.Y. Tey, Combination of ultrasonication and deep eutectic solvent in pretreatment of lignocellulosic biomass for enhanced enzymatic saccharification, *Cellulose*. (2021). <https://doi.org/10.1007/s10570-020-03598-5>.
- [47] T. Leong, M. Ashokkumar, S. Kentish, The fundamentals of power ultrasound - A Review, *Acoustics Australia*. 39 (2011) 54–63. <https://doi.org/10.1118/1.3611561>.
- [48] S.J. Lighthill, Acoustic streaming, *Journal of Sound and Vibration*. 61 (1978) 391–418. [https://doi.org/10.1016/0022-460X\(78\)90388-7](https://doi.org/10.1016/0022-460X(78)90388-7).
- [49] W.Y. Tey, A. Yutaka, C.S. Nor Azwadi, R.Z. Goh, Governing equations in computational fluid dynamics: Derivations and a recent review, *Progress in Energy and Environment*. 1 (2017) 1–19. <http://www.akademiabaru.com/submit/index.php/progee/article/view/1026>.
- [50] Q. Tang, J. Hu, S. Qian, X. Zhang, Eckart acoustic streaming in a heptagonal chamber by multiple acoustic transducers, *Microfluidics and Nanofluidics*. 21 (2017). <https://doi.org/10.1007/s10404-017-1871-1>.
- [51] C. Eckart, Vortices and Streams Caused by Sound Waves, *Physical Review*. 73 (1948) 68–76. <https://doi.org/10.1103/PhysRev.73.68>.
- [52] A.J. Sojahrood, H. Haghi, Q. Li, T.M. Porter, R. Karshafian, M.C. Kolios, Nonlinear power loss in the oscillations of coated and uncoated bubbles: Role of thermal, radiation and encapsulating shell damping at various excitation pressures, *Ultrasonics Sonochemistry*. 66 (2020) Article 105070. <https://doi.org/10.1016/j.ultsonch.2020.105070>.



- [53] Y. Zhang, S. Yuan, L. Wang, Investigation of capillary wave, cavitation and droplet diameter distribution during ultrasonic atomization, *Experimental Thermal and Fluid Science*. 120 (2021) Article ID 110219. <https://doi.org/10.1016/j.expthermflusci.2020.110219>.
- [54] R. Dewil, J. Baeyens, R. Goutvriend, Use of ultrasonics in the treatment of waste activated sludge, *Chinese Journal of Chemical Engineering*. 14 (2006) 105–113. [https://doi.org/10.1016/S1004-9541\(06\)60045-1](https://doi.org/10.1016/S1004-9541(06)60045-1).
- [55] B. Helfield, J.J. Black, B. Qin, J. Pacella, X. Chen, F.S. Villanueva, Fluid Viscosity Affects the Fragmentation and Inertial Cavitation Threshold of Lipid-Encapsulated Microbubbles, *Ultrasound in Medicine & Biology*. 42 (2016) 782–794. <https://doi.org/10.1016/j.ultrasmedbio.2015.10.023>.
- [56] I. Tzanakis, G.S.B. Lebon, D.G. Eskin, K.A. Pericleous, Characterizing the cavitation development and acoustic spectrum in various liquids, *Ultrasonics Sonochemistry*. 34 (2017) 651–662. <https://doi.org/10.1016/j.ultsonch.2016.06.034>.
- [57] S. Muthukumar, S.E. Kentish, G.W. Stevens, M. Ashokkumar, Application of ultrasound in membrane separation processes: A review, *Reviews in Chemical Engineering*. 22 (2006). <https://doi.org/10.1515/REVCE.2006.22.3.155>.
- [58] L.A. Crum, Comments on the evolving field of sonochemistry by a cavitation physicist, *Ultrasonics Sonochemistry*. 2 (1995) S147–S152. [https://doi.org/10.1016/1350-4177\(95\)00018-2](https://doi.org/10.1016/1350-4177(95)00018-2).
- [59] G. Zhang, P. Zhang, J. Gao, Y. Chen, Using acoustic cavitation to improve the bio-activity of activated sludge, *Bioresource Technology*. 99 (2008) 1497–1502. <https://doi.org/10.1016/j.biortech.2007.01.050>.
- [60] M. Ashokkumar, The characterization of acoustic cavitation bubbles - An overview, *Ultrasonics Sonochemistry*. 18 (2011) 864–872. <https://doi.org/10.1016/j.ultsonch.2010.11.016>.
- [61] A. Iskalieva, B.M. Yimmou, P.R. Gogate, M. Horvath, P.G. Horvath, L. Csoka, Cavitation assisted delignification of wheat straw: A review, *Ultrasonics Sonochemistry*. 19 (2012) 984–993. <https://doi.org/10.1016/j.ultsonch.2012.02.007>.
- [62] J. Luo, Z. Fang, R.L. Smith, Ultrasound-enhanced conversion of biomass to biofuels, *Progress in Energy and Combustion Science*. 41 (2014) 56–93. <https://doi.org/10.1016/j.pecs.2013.11.001>.
- [63] A. Tiehm, K. Nickel, M. Zellhorn, U. Neis, A. Tiehm, Ultrasonic waste activated sludge disintegration for improving anaerobic stabilization, *Water Research*. 35 (2001) 2003–2009. [https://doi.org/10.1016/S0043-1354\(00\)00468-1](https://doi.org/10.1016/S0043-1354(00)00468-1).
- [64] N.P. Vichare, P. Senthilkumar, V.S. Moholkar, P.R. Gogate, A.B. Pandit, Energy analysis in acoustic cavitation, *Industrial and Engineering Chemistry Research*. 39 (2000) 1480–1486. <https://doi.org/10.1021/ie9906159>.
- [65] N.N. Mahamuni, Y.G. Adewuyi, Optimization of the synthesis of biodiesel via ultrasound-enhanced base-catalyzed transesterification of soybean oil using a multifrequency ultrasonic reactor, *Energy and Fuels*. 23 (2009) 2757–2766. <https://doi.org/10.1021/ef900047j>.
- [66] L. Cherpozat, E. Loranger, C. Daneault, Ultrasonic pretreatment of soft wood biomass prior to conventional pyrolysis: Scale-up effects and limitations, *Biomass and Bioenergy*. 124 (2019) 54–63. <https://doi.org/10.1016/j.biombioe.2019.03.009>.
- [67] N.T. Le, C. Julcour-Lebigue, H. Delmas, An executive review of sludge pretreatment by sonication, *Journal of Environmental Sciences (China)*. 37 (2015) 139–153. <https://doi.org/10.1016/j.jes.2015.05.031>.
- [68] R. Sivaramakrishnan, A. Incharoensakdi, Microalgae as feedstock for biodiesel production under ultrasound treatment – A review, *Bioresource Technology*. 250 (2018) 877–887. <https://doi.org/10.1016/j.biortech.2017.11.095>.
- [69] M. Kurokawa, P.M. King, X. Wu, E.M. Joyce, T.J. Mason, K. Yamamoto, Effect of sonication frequency on the disruption of algae, *Ultrasonics Sonochemistry*. 31 (2016) 157–162. <https://doi.org/10.1016/j.ultsonch.2015.12.011>.
- [70] D. Nagarajan, J.S. Chang, D.J. Lee, Pretreatment of microalgal biomass for efficient biohydrogen production – Recent insights and future perspectives, *Bioresource Technology*. 302 (2020) Article ID 122871. <https://doi.org/10.1016/j.biortech.2020.122871>.
- [71] K.J.Y. Chong, C.Y. Quek, F. Dzaharudin, A. Ooi, R. Manasseh, The effects of coupling and bubble size on the dynamical-systems behaviour of a small cluster of microbubbles, *Journal of Sound and Vibration*. 329 (2010) 687–699. <https://doi.org/10.1016/j.jsv.2009.09.037>.

## Appendix

Shockwave pressure  $P_{shock}$ , collapsing temperature  $T_{collapse}$ , and collapsing pressure  $P_{collapse}$  of microbubble due to various operating conditions.

Set	$\sigma_s$ (N/m)	$\mu$ (Pa.s)	$f$ (kHz)	$W$ (W)	$u_{max}$ (m/s)	$P_{shock}$ (GPa)	Radius Ratio	$T_{collapse}$ (K)	$P_{collapse}$ (GPa)
1	$50 \times 10^{-3}$	$0.8 \times 10^{-3}$	80	400	1513.6420	6.8887	59.7800	2952.7843	2719.6195
2	$100 \times 10^{-3}$	$0.8 \times 10^{-3}$	80	400	3679.2917	20.3916	90.9694	4886.9703	15861.1999
3	$150 \times 10^{-3}$	$0.8 \times 10^{-3}$	80	400	6935.2433	51.6906	122.8411	7007.7305	56003.8617
4	$200 \times 10^{-3}$	$0.8 \times 10^{-3}$	80	400	11287.6811	125.0105	154.7778	9247.3084	147825.9936
5	$250 \times 10^{-3}$	$0.8 \times 10^{-3}$	80	400	16725.5812	303.8145	186.5493	11569.5718	323822.9322
6	$300 \times 10^{-3}$	$0.8 \times 10^{-3}$	80	400	23231.9713	762.8196	218.0639	13952.9386	623773.6096
7	$350 \times 10^{-3}$	$0.8 \times 10^{-3}$	80	400	30788.0537	2010.5116	249.2870	16383.4252	1094242.466
8	$200 \times 10^{-3}$	$0.2 \times 10^{-3}$	80	400	21048.0219	629.0354	207.7493	14616.4647	565029.3215
9	$200 \times 10^{-3}$	$0.4 \times 10^{-3}$	80	400	16961.1811	337.9104	187.5754	12502.1383	355730.9192
10	$200 \times 10^{-3}$	$0.6 \times 10^{-3}$	80	400	13531.2619	190.5526	168.5787	10621.9827	219393.4087
11	$200 \times 10^{-3}$	$0.8 \times 10^{-3}$	80	400	11287.6811	125.0104	154.7778	9247.3084	147825.9936
12	$200 \times 10^{-3}$	$1.0 \times 10^{-3}$	80	400	8841.9445	75.5054	137.9533	7758.5245	87818.319
13	$200 \times 10^{-3}$	$1.2 \times 10^{-3}$	80	400	6847.8719	46.9127	122.3318	6460.2684	50989.2204
14	$200 \times 10^{-3}$	$1.4 \times 10^{-3}$	80	400	4905.4985	27.0446	104.5930	5140.734	25359.6336
15	$200 \times 10^{-3}$	$0.8 \times 10^{-3}$	20	400	10380.9382	120.456	148.7470	10031.9343	236129.6771
16	$200 \times 10^{-3}$	$0.8 \times 10^{-3}$	40	400	10681.0340	124.2831	150.7725	9949.0399	207653.09
17	$200 \times 10^{-3}$	$0.8 \times 10^{-3}$	60	400	10983.2952	125.9274	152.7826	9690.0997	177804.1303
18	$200 \times 10^{-3}$	$0.8 \times 10^{-3}$	80	400	11287.6811	125.0104	154.7778	9247.3084	147825.9936
19	$200 \times 10^{-3}$	$0.8 \times 10^{-3}$	100	400	11594.1522	121.1156	156.7584	8612.934	118822.7337
20	$200 \times 10^{-3}$	$0.8 \times 10^{-3}$	120	400	11902.6711	113.7865	158.7247	7779.3155	91722.8065
21	$200 \times 10^{-3}$	$0.8 \times 10^{-3}$	140	400	12213.1998	102.5228	160.6771	6738.861	62140.7436
22	$200 \times 10^{-3}$	$0.8 \times 10^{-3}$	80	100	10681.0159	111.9388	150.7723	8960.8876	132411.4985
23	$200 \times 10^{-3}$	$0.8 \times 10^{-3}$	80	200	10931.2658	117.2000	152.4387	9079.8603	138667.3396
24	$200 \times 10^{-3}$	$0.8 \times 10^{-3}$	80	300	11124.2887	121.3827	153.7103	9170.8304	143591.0676
25	$200 \times 10^{-3}$	$0.8 \times 10^{-3}$	80	400	11287.6811	125.0104	154.7778	9247.3084	147825.9936
26	$200 \times 10^{-3}$	$0.8 \times 10^{-3}$	80	500	11432.1332	128.2853	155.7148	9314.5268	151621.1849
27	$200 \times 10^{-3}$	$0.8 \times 10^{-3}$	80	600	11563.1285	131.3111	156.5591	9375.1695	155104.3743
28	$200 \times 10^{-3}$	$0.8 \times 10^{-3}$	80	700	11683.9245	134.1492	157.3333	9430.8299	158351.3584